

1995122421

N95-28842

A STUDY OF STRUCTURALLY EFFICIENT GRAPHITE-THERMOPLASTIC
TRAPEZOIDAL-CORRUGATION SANDWICH AND SEMI-SANDWICH PANELS

Dawn C. Jegley
NASA Langley Research Center
Hampton, VA

519-24
51419

ABSTRACT

The structural efficiency of compression-loaded trapezoidal-corrugation sandwich and semi-sandwich composite panels is studied to determine their weight savings potential. Sandwich panels with two identical face sheets and a trapezoidal corrugated core between them, and semi-sandwich panels with a corrugation attached to a single skin are considered. An optimization code is used to find the minimum weight designs for critical compressive load levels ranging from 3,000 to 24,000 lb/in. Graphite-thermoplastic panels based on the optimal minimum weight designs were fabricated and tested. A finite-element analysis of several test specimens was also conducted. The results of the optimization study, the finite-element analysis, and the experiments are presented.

INTRODUCTION

The high stiffness, high strength, low density, and tailorability of composite materials has greatly increased the potential for designing structures which are more efficient than metallic structures. An important consideration in designing these structures is the cost involved in their manufacturing. To make composite structures a viable replacement for metallic structures, composite structures must be designed to take advantage of cost-effective manufacturing techniques in order to minimize their cost.

A cost-effective manufacturing technique that is receiving attention is thermoforming. A structural concept that can exploit thermoforming is a panel with one or two face sheets and a trapezoidal-shaped corrugated core. This structural concept is attractive since the trapezoidal corrugation can be thermoformed from one continuous constant-thickness graphite-thermoplastic sheet of material and consolidated into a sandwich panel with two face sheets or a semi-sandwich panel with one face sheet. The manufacturing process involves thermoforming these large sheets of composite material with metal tools after the sheets have been laid up in the appropriate stacking sequence. Since the corrugated sheet is initially a continuous flat sheet, it is relatively easy to fabricate these panel elements into the desired shape. The corrugations require no additional cutting or aligning, thereby requiring less effort to construct than discrete stiffeners. However, one drawback to this technique is that thermoforming can impose restrictions on the design if a constant thickness corrugation is required.

For panels of this type to be used in aircraft structures, they must be structurally efficient, easily manufacturable, and their behavior must be predictable. The present study focuses on examining the response of thermoformed sandwich and semi-sandwich panels with a trapezoidal corrugation. An analytical

optimization study was conducted to identify structurally efficient designs for panels subjected to compressive loads. Results of this study are presented herein. Based on optimal designs, representative panels were fabricated and tested. The results of these tests and of a corresponding finite-element analysis are presented in the present paper.

PANEL CONFIGURATIONS AND STRUCTURAL EFFICIENCY CALCULATIONS

Two panel configurations were considered in this study. The first configuration is a semi-sandwich panel with a trapezoidal-shaped continuous corrugation attached to a single face sheet. A cross-section of a semi-sandwich panel is shown in figure 1(a). The second configuration is a sandwich panel with a trapezoidal-shaped continuous corrugation attached to two identical face sheets. A cross-section of a sandwich panel is shown in figure 1(b).

Structurally efficient designs were determined for sandwich and semi-sandwich panels with trapezoidal corrugations. The optimal (minimum weight) configurations were determined and evaluated using the computer code PASC0 (ref. 1). The design variables were ply thicknesses and corrugation dimensions (see figure 1). Optimum panels for each configuration were designed to support axial compressive loads corresponding to N_x/L (where N_x is the axial stress resultant and L is the panel length) of 100, 250, 500 and 800 lb/in². No lateral or shear loading was considered.

Allowable stacking sequences contained only $\pm 45^\circ$, 0° and 90° -degree plies. Design constraints are given in table I and include maximum allowable strains and minimum ply thicknesses on the outermost $+45^\circ$ -degree and -45° -degree plies. The angle between the skin and the sides of the corrugation (see figure 1) was required to be 45 degrees and the skin was assumed to be flat. For the optimization process, all panels were designed to be 30 inches long and 24 inches wide and the material properties for a typical graphite-thermoplastic material given in table II were used. These properties accurately represent the experimentally determined properties of flat graphite-thermoplastic panels as shown in reference 2. Initially, no restrictions were placed on corrugation width (shown as b in figure 1). Minimum overall extensional and shear stiffness constraints, as given in reference 3, were also included. All panels were designed to be buckling critical; however, the buckling loads determined by PASC0 are based on the assumption that no out-of-plane prebuckling deformations are present.

SPECIMENS, APPARATUS AND TESTS

Panel Configurations

Six panels were fabricated from Hercules AS4 graphite fiber and ICI PEEK thermoplastic resin, and are described in table III. In each panel, the $\pm 45^\circ$ -degree plies were made with woven fabric and all other plies were made from unidirectional tape. Four types of semi-sandwich panels and two types of sandwich panels were constructed. The panel designs were based on the PASC0 optimization results but significant changes were made to the optimum designs to provide a more realistic design. Changes to the PASC0 designs included increasing layer thickness to obtain an integral number of plies (i.e., fractions of plies were rounded up or down), forcing all laminates to

be balanced (PASCO requires symmetric laminates) and requiring at least one 90-degree ply in each laminate. The stacking sequences and dimensions of each fabricated panel are shown in table III. Semi-sandwich panels are identified as panels A, B, C, and D. Sandwich panels are identified as panels E and F.

The semi-sandwich panels were constructed with one flat skin and a corrugation and were placed in the autoclave for consolidation. However, when the panels cooled to room temperature, the skin of the semi-sandwich panels deformed out-of-plane into a cylindrical surface. A photograph of the cross-section of panel A is shown in figure 2(a). The amount of curvature of the skin was measured for each panel prior to testing. The variation of the skin from a flat surface (designated as h in figure 2) was .85, .42, .48 and .22 inches for panels A, B, C, and D, respectively. The maximum curvature was in panel A and this curvature corresponds to an equivalent cylinder with radius of curvature of the skin of 91 inches. The sandwich panels did not deform out-of-plane during the fabrication or cooling processes and were essentially flat. A photograph of the cross-section of panel E is shown in figure 2(b).

Prior to compression testing, one inch of each end of each panel was potted in an epoxy compound and the potted ends were ground flat and parallel. The semi-sandwich panels were not flattened to remove the curvature prior to potting the ends. Strain gages were bonded to each panel. The semi-sandwich panels had strain gages on the skin and corrugations while the sandwich panels only had gages on the skins since the corrugation was not accessible for gage application. The skin of each semi-sandwich panel and one skin of each sandwich panel was painted white to produce a reflective surface so moiré interferometry could be used to monitor out-of-plane deformations during the test.

Panel Properties

Two flat coupons 1.5 inches wide, 2 inches long and approximately 0.2 inches thick were cut from sandwich panel E after the panel was tested. The coupons were cut from a section of the panel where the corrugation was attached to the skin and where post-failure ultrasonic C-scan inspection indicated that no damage was present. These coupons were loaded in axial compression while the end-shortening displacement was recorded to determine the stiffness of the coupon. Flat coupons could not be cut from the semi-sandwich panels so coupons cut from panel E are assumed to be representative of all panels tested. Stiffnesses of these coupons were calculated based on load-end-shortening results from the compression tests. Stiffness predictions were also calculated using laminate theory and finite-element analysis with the typical graphite-thermoplastic material properties given in table II. A comparison of the assumed and experimentally determined stiffnesses indicates that the assumed material properties for typical graphite-thermoplastic materials were approximately 25% too high to accurately represent the coupons and the panels tested. Therefore, the experimentally determined stiffness values were used for the finite-element analysis of the test specimens. Equivalent lamina properties corresponding to these stiffnesses are shown in table II. No allowance is made for the fact that all ± 45 degree plies were made from woven fabric in all panels tested. These layers are assumed to be tape layers in the analysis (i.e., no fiber undulations were considered). Each flat coupon was measured and weighed prior to testing to determine the density. The assumed density was accurate.

Apparatus and Testing

All panels were slowly loaded to failure in axial compression in a 1.2 Mlb-capacity hydraulic testing machine. Unloaded edges were unsupported. Strain gage data and out-of-plane deformations at selected locations and panel end-shortening displacements were recorded during the test. Moiré fringe patterns were photographed and video taped during the test.

FINITE-ELEMENT ANALYSIS

A nonlinear finite-element analysis of each panel was conducted using the STAGS computer code (ref. 4). Actual stacking sequences, measured thicknesses and corrugation dimensions were used for the analytical model. All plies within a laminate were assumed to be the same thickness, with a woven ± 45 layer assumed to be the thickness of two plies. All corrugations were assumed to be identical within a given panel. The entire panel was modeled and the overall panel curvature was included as an initial geometric imperfection. The section of each panel in the potting compound was included in the analytical model and no out-of-plane or lateral deformations were permitted in this region. The unloaded edges of the panel were unrestrained. Four-noded quadrilateral elements were used to model the panels. A uniform grid was implemented along the length of the panel with each element being one inch long for panels A, B, C, D and F. Elements which were 0.5 inches long were used to model panel E. These models involved 6,000 to 10,000 degrees of freedom, depending upon panel geometry. The element width varied depending on panel configuration. The boundary conditions for a semi-sandwich panel are shown in figure 3.

One semi-sandwich panel was modeled with 1-inch-long elements and with .5-inch-long elements to determine if a converged solution had been obtained. Less than one percent difference was found in the end-shortening, prebuckling and postbuckling out-of-plane displacements or eigenvalues from the analyses based on 1-inch-long elements and on 0.5-inch-long elements.

The prebuckling stiffness, prebuckling out-of-plane deformation shape and buckling load were determined for each panel based on a nonlinear prebuckling stress state. For panels A and E the analysis was continued for loading beyond the buckling load. Nonlinear analysis for the postbuckling response was conducted using the eigenvector corresponding to the lowest eigenvalue to represent an initial geometric imperfection and to initiate the analysis to determine postbuckling deformation shape and postbuckling stiffness.

RESULTS AND DISCUSSION

Optimized Panel Designs

Optimum designs for semi-sandwich and sandwich panels are presented in this section for a variety of design constraints. In all cases, all four edges of the panel were assumed to be simply supported (PASCO requires simply supported loaded edges) and all corrugations within a panel were assumed to be identical. The initial design imposed no restrictions on the number of corrugations across the panel width

of approximately 24 inches. However, in each case, the optimum design resulted in five corrugations. Since final optimal designs required exactly a 24-inch width, five 4.8-inch-wide corrugations were required. The skin of the panel was assumed to be flat prior to loading for all designs.

The structural efficiency of optimal panel designs were determined assuming the typical material properties of graphite-thermoplastic material shown in table II. The structural efficiency results are shown in figure 4 in the form of a weight index W/AL (where W is the panel weight, A is the panel planform area and L is the panel length) versus a load index N_x/L . Results are presented in this manner for ease of comparison with results presented in the literature such as in references 3 and 5. The solid lines represent optimum semi-sandwich panels and the dashed lines represent optimum sandwich panels. The most structurally efficient configurations are those represented by the lowest curves on the plot, which are those designs with the lowest weight index for a specified load index. The lowest dashed and solid curves on the plot were determined using the constraints listed in table I. Laminate thicknesses and corrugation width of optimum panel designs found by using the constraints in table I are given in table IV.

Practical designs would include additional restrictions not included in table I. Examples of such restrictions would be an additional requirement of one 90-degree ply in each laminate and requiring an integral number of plies of each orientation. These additional restrictions were imposed on the designs and the results are also shown in figure 4. These additional requirements increased the weight of each designed panel by 4 to 13 percent above the optimum weight when these additional constraints were not included. Also shown on the figure is the structural efficiency of typical aluminum aircraft panels, represented by the shaded region. The results indicate that the graphite-thermoplastic panels are significantly more structurally efficient than the aluminum panels for all load levels considered. The results also indicate that there is little difference between the structural efficiency of the semi-sandwich and sandwich panels. The results also indicate that additional constraints which might be required to make the panel designs more practical, such as including a minimum number of 90-degree plies and an integral number of plies, do not significantly reduce the panel's structural efficiency.

Critical constraints of optimum-design panels are dependent upon design load level and are given in table IV. Extensional stiffness is a critical constraint in all panels except the most heavily loaded semi-sandwich panel. Shear stiffness is critical in all semi-sandwich panels. PASCO cannot calculate an overall shear stiffness for sandwich panels so no overall shear stiffness requirement was imposed on the sandwich panel design, hence, overall shear stiffness could not be critical. At least one buckling mode is also critical for each panel. Allowable inplane shear strain is a critical constraint for the most heavily loaded semi-sandwich panel. Optimum corrugation width decreases and height increases as load level increases. The optimal thickness of the ± 45 - and 0-degree plies depends on load level. The lightest weight panel designs have no 90-degree plies. For the lowest load level considered, the thickness of the ± 45 -degree plies is the minimum thickness allowed.

The structural efficiency of optimal panel designs in which the constraints in table I were used are shown again in figure 5. The structural efficiency of optimal panel designs that include all constraints in table I except those on minimum overall stiffnesses and minimum thickness of exterior ± 45 -degree plies are also shown in figure 5. Removing these constraints reduces the weight of the lightly-loaded semi-sandwich panels significantly and has a small effect on the sandwich panel weights.

The minimum thickness constraint has little effect on the heavily-loaded panels so there is little difference between the heavily-loaded semi-sandwich panels and there is no difference between the heavily-loaded sandwich panels. Sandwich panels are not as structurally efficient as semi-sandwich panels in some cases because both skins in each sandwich panel were required to be identical, resulting in increased weight.

A comparison between the PASCO and finite-element models and results was conducted for a heavily-loaded semi-sandwich panel by comparing the critical buckling loads predicted by PASCO and by STAGS using the method described in reference 6. This comparison is only used for model verifications since the allowable boundary conditions in PASCO do not accurately reflect test conditions, since PASCO does not allow for any prebuckling deformations, and since panel skin curvature is not included in the PASCO analysis. Buckling loads predicted by PASCO and by STAGS for this case differ by less than 5 percent.

Fabricated Panels

The panels described in table III and figures 1 and 2 were loaded to failure in axial compression. A comparison of the test and finite-element results of the panels is presented in this section. A comparison of W/A and N_x of tested panels indicates that the graphite-thermoplastic panels weigh approximately half the weight of aluminum panels designed to support the same load.

The test specimens described in this section exhibit nonlinear prebuckling deformations. This result is substantiated by the presence of moiré fringe patterns at low load levels that indicate out-of-plane deformations in the specimen skins. Moreover, the semi-sandwich specimens inherently have load path eccentricity. When these deformation characteristics are present, the onset of buckling is difficult to identify experimentally. Therefore, experimental buckling loads are not presented herein. Analytical buckling loads for the test specimens were obtained using finite-element analysis. The results are used in the present study to provide insight into the test results. For example, results are presented in figure 6 that show the values of the axial stress resultant N_x in the specimens at failure, represented by bars in the figure. Analytical predictions of buckling are also shown, represented by symbols. These results suggest that panels B and D failed prior to buckling and that the remaining panels supported load into the postbuckling region. To gain further insight into panel behavior, selected postbuckling analyses were conducted. A discussion of the test results for each of the panels is presented subsequently.

Semi-sandwich Panels

The semi-sandwich specimens exhibited noticeable out-of-plane deformation at low load levels. These deformations were detected using moiré interferometry. However, the load versus end-shortening curves were linear over most of the load range prior to failure, and gave no indication of a stiffness change associated with an overall general instability type of buckling response. To gain insight into panel response, buckling and postbuckling finite-element analyses were conducted. The presence of out-of-plane deformations in the test specimens at low load levels motivated the use of buckling analyses that include nonlinear prebuckling deformations.

For panel A, the global axial stiffness predicted by finite-element analysis is 3 percent less than that of the test specimen. The buckling analysis predicted a localized mode with out-of-plane deformations only in one corner of the panel. Postbuckling analysis indicated a change in the global axial stiffness of less than

one percent, which is consistent with the experimental data, and the presence of local regions of out-of-plane deformation. A contour plot of the predicted nonlinear out-of-plane prebuckling deformation pattern at a load of 97 percent of the predicted buckling load is shown in figure 7(a). A similar plot of the postbuckling deformation pattern at a load of 169 percent of the predicted buckling load is shown in figure 7(b). These results indicate that the nonlinear prebuckling deformation and postbuckling deformation patterns are very similar in shape and that the bending gradients are much more pronounced in the postbuckling range. The center of the panel has an out-of-plane deformation of .06 in. at $P/P_{cr}=0.97$ and .078 in. at $P/P_{cr}=1.69$, which is just before failure. Both of these deformations are larger than the skin thickness and indicate the presence of large nonlinear bending gradients. Photographs of the panel, showing moiré patterns of out-of-plane deformations, are shown in figures 8(a) and 8(b) for load levels approximately 95 percent and 170 percent of the predicted buckling load, respectively. These moiré patterns agree with the analytically determined patterns. Out-of-plane deformations in panel A are generally confined to regions of the skin where it is not attached to the corrugation and regions near the free edge.

Maximum strains occur in the skin under the corrugation nearest each free edge. The maximum axial and lateral strains occur near the horizontal center of the panel and have values of -.0055 and .0032 in./in., respectively. Maximum shear strains occur at the edge of the potting and have values of ± 0.0022 in./in. Separation at the interface between the skin and corrugation caused the failure of panel A. As the amplitude of the out-of-plane deformation grew, high strains developed in the skin (at the center of the panel, strain gages indicated the axial strain was -.0055 in./in. and the lateral strain was .0070 in./in. at failure) and deformations caused separation at points where the corrugation meets the skin. A sketch of the initial and deformed cross-section of panel A is shown in figure 9 (with the magnitude of the deformations amplified). Separation occurred at points labeled A on the sketch. The largest deformations are located in the regions of the skin not attached to the corrugation. Also influencing strains in the panel is the difference in Poisson's ratios between the skin and corrugation. This difference can be expressed as a ratio of the values of the Poisson's ratios in the skin to the value of the Poisson's ratios in the corrugation, as calculated using laminate analysis. In panel A these ratios are $\nu_{xy}(\text{skin})/\nu_{xy}(\text{corrugation})=1.3$ and $\nu_{yx}(\text{skin})/\nu_{yx}(\text{corrugation})=6.4$. The further these ratios are from 1 (which would represent two laminates with the same Poisson's ratios), the larger the mismatch in properties and the larger the interlaminar stresses which develop during loading. This mismatch causes the skin and corrugation to try to deform different amounts even though they are bonded together and must maintain deformation compatibility. These resulting high interlaminar stresses eventually result in separation between the skin and the corrugation. A photograph of panel A after failure is shown in figure 10.

To examine the local deformations under the corrugation, a finite-element analysis of a panel with only one corrugation was conducted. Since the panel skin is less than .05 inches thick and contains only one 90-degree ply, little lateral load is required to induce out-of-plane deformations in the thin skin. Analysis indicates that, away from the clamped edges, an applied compressive axial stress resultant induces a tensile lateral stress resultant which is 10 percent of the magnitude of the axial stress resultant. However, near the clamped edges the applied compressive axial stress resultant induces a compressive lateral stress resultant 60 percent as large as the axial stress resultant. This compressive lateral stress causes local out-of-plane deformations at the clamped ends, as seen in the tested panel.

Panel B also exhibited out-of-plane deformations at very low load levels, but the deformation pattern was different from that in panel A. Prebuckling stiffness predicted by analysis is 3 percent higher than the stiffness found from experiment. The finite-element prediction of prebuckling deformation at $P/P_{cr}=.75$ is shown in figure 11, where P_{cr} is the buckling load predicted by finite-element analysis. No local deformations or high bending gradients of the type seen in panel A are present. Axial strain gages indicated strains of $-.0056$ in./in. at failure. Finite-element analysis also indicates high axial strain levels at the failure load. Initial failure appears to cause a sudden increase in strain in the corrugation leading to separation between the corrugation and skin. A photograph of panel B after failure is shown in figure 11(b). The skin and corrugation have separated over a large section of the panel. The difference in Poisson's ratios between the skin and corrugation is less than in panel A. The ratios of the Poisson's ratios are $\nu_{xy}(\text{skin})/\nu_{xy}(\text{corrugation})=.91$ and $\nu_{yx}(\text{skin})/\nu_{yx}(\text{corrugation})=.21$, in panel B. The panel failed at $P/P_{cr}=.88$.

Out-of-plane deformations at very low load levels also occurred in panels C and D. Analytically determined prebuckling deformations at $P/P_{cr}=.95$ in panel C and at $P/P_{cr}=.88$ in panel D are shown in figures 12 and 13, respectively. A deformation shape resembling one half-wave in each direction occurred in panel C just prior to failure. A deformation shape resembling that found in panel B occurred in panel D, with the out-of-plane deformation at the unsupported edges opposite in sign from the deformation at the center of the panel. Deformations in panels B and D were not limited to the thin section of skin between the corrugations.

The strain gages at the horizontal centerline of panel C indicated a maximum axial strain of approximately $-.0055$ in./in. prior to failure. Strain gages on panel D indicated a maximum failure strain of $-.0048$ in./in. at the panel horizontal centerline on the corrugation. Panels C and D failed across the corrugation midlength and the corrugation separated from the skin but little damage in the skin due to panel failure could be seen. The separation between the corrugation and the skin was only at the corrugation-skin interface in panel C. However, plies from the skin stuck to the corrugation and vice versa in panel D. Little damage to the skin could be seen after loading was removed from panels C and D. The ratio the skin and corrugation Poisson's ratios is $\nu_{xy}(\text{skin})/\nu_{xy}(\text{corrugation})=1.87$ and $\nu_{yx}(\text{skin})/\nu_{yx}(\text{corrugation})=5.6$, in panel C and 1.41 and 2.21, respectively, in panel D.

Sandwich Panels

Panels E and F also exhibited out-of-plane deformation at very low load levels, however, the magnitude of this deformation remained quite small throughout loading. Predicted and experimental prebuckling stiffnesses differ by less than one percent in panel E but differ by 12 percent in panel F. Predicted and experimental postbuckling stiffnesses differ by 4 percent in panel E.

According to the analysis of panel E, the sections of skin not attached to the corrugations deform prior to buckling, as shown in the contour plot of out-of-plane deformation in figure 14(a). The prebuckling deformation pattern resembles one axial half-wave under each center corrugation. However, the maximum magnitude of the prebuckling deformations is less than one ply thickness. The deformations shown correspond to 94 percent of the predicted buckling load. Moiré patterns indicate that the center sections of thin skin in panel E deform into a pattern resembling two axial half-waves. However, the skin of the panel was only .05 inches thick and the

predicted deformation in this region is so small that any imperfection in this section of skin could cause an unexpected deformation shape.

Predicted postbuckling deformations are shown in figure 14(b) for 161 percent of the predicted buckling load. This load corresponds to a value just below that of test specimen failure. Loading was stopped when the attempt to increase load resulted in increased end-shortening and a reduction in load carrying capability. The failure load was defined as the maximum load level reached. Strains in the panel skins were calculated for this load level. At the maximum load, large deformations occur near the free edges of both skins. The magnitude of the deformations are indicated on the figure. The maximum axial and shear strains, $-.0050$ and $-.0025$ in./in., respectively, occur near the corners of one skin of the panel. Panel E was ultrasonically inspected by C-scan after testing to determine where damage had occurred since no damage was visible after the panel was removed from the test machine. C-scan inspection indicated that the only damaged region of the panel is a separation between the skin and corrugation at the location of maximum axial and shear strains. The mismatched Poisson ratios between the skin and corrugation can be expressed as $\nu_{xy}(\text{skin})/\nu_{xy}(\text{corrugation})=1.11$ and $\nu_{yx}(\text{skin})/\nu_{yx}(\text{corrugation})=7.79$ in panel E. According to the analysis, when panel E reaches a load of $P/P_{cr}=1.8$, the end-shortening rapidly grows with slight increases in load, indicating that panel failure would occur.

Panel F behaved in a manner similar to panel E; however, each thin section of skin initially deformed into two axial half-waves and then the entire panel buckled into a one axial half-wave. The deformation patterns predicted by analysis indicate out-of-plane prebuckling deformations of $.07$ inches at the free edges and $.045$ inches in the skin at the center of the panel at a load of 95 percent of the buckling load. The value of $.045$ inches agrees with the experimentally measured value but no measurements were recorded during testing at the panel's unsupported edges. This maximum deformation prior to buckling is larger than the skin thickness. This panel failed by shortening rapidly without additional increase in load, but with no visible damage after loading reached a maximum value. C-scan inspection indicated extensive damage near one potted end in a region several inches long and about ten inches wide. When panel F reaches $P/P_{cr}=.99$, the end-shortening rapidly grows and the panel fails. The Poisson's ratios in panel F are the same as those in panel E since the only difference between the panels is length.

CONCLUDING REMARKS

The potential of structurally efficient graphite-thermoplastic panels for aircraft components that were fabricated using the thermoforming technique was examined. Thermoforming can be used to fabricate trapezoidal-corrugation sandwich and semi-sandwich panels which consist of a continuous corrugation and two or one face sheets, respectively. An optimization study indicates that minimum-weight trapezoidal-corrugation sandwich and semi-sandwich composite panels are more structurally efficient than current aluminum wing compression panels used on aircraft today. However, semi-sandwich panels are likely to deform out-of-plane during the fabrication process, which must be taken into account in any design. Testing of semi-sandwich panels identified a nonlinear displacement behavior, so a finite-element analysis based on a nonlinear prebuckling stress state was conducted. This analysis accurately predicts panel deformations and strains caused by axial compressive loading. Analysis indicates that significant prebuckling out-of-plane

deformations occurred in all semi-sandwich panels, as shown by moiré patterns of test specimens under load. Sandwich panels did not deform out-of-plane during fabrication and did not display as much nonlinear behavior as the semi-sandwich panels. Failure of each panel involved separation of the corrugation from the skin either near the clamped edge or midlength but always across the entire panel width.

This study indicates that the thermoforming technique can be used to build structurally efficient graphite-thermoplastic panels and that the prebuckling and postbuckling behavior of these panels can be accurately predicted. Thermoforming is a viable manufacturing technique worthy of further consideration.

REFERENCES

1. Anderson, Melvin S.; and Stroud, W. Jefferson: A General Panel Sizing Computer Code and Its Applications to Composite Structural Panels. AIAA Journal, Vol. 17., No. 8, August 1979, pp. 892-897.
2. Jegley, Dawn C.: Compression Behavior of Graphite-Thermoplastic and Graphite-Epoxy Panels with Circular Holes or Impact Damage. NASA TP-3071, March 1991.
3. Williams, J. G.; Anderson, M. S.; Rhodes, M. D.; Starnes, J. H., Jr.; and Stroud, W. J.: Recent Developments in the Design, Testing, and Impact-Damage Tolerance of Stiffened Composite Panels, Fibrous Composites in Structural Design (Proceedings of Fourth Conference on Fibrous Composites in Structural Design), Plenum Press, New York, 1980, pp. 259-291.
4. Almroth, B. O.; and Brogan, F. A.: The STAGS Computer Code. NASA CR-2950, 1980.
5. Williams, Jerry G.; and Mikulas, Martin M., Jr.: Analytical and Experimental Study of Structurally-Efficient Composite Hat-Stiffened Panels Loaded in Axial Compression. NASA TM X-72813, 1976.
6. Stroud, W. Jefferson; Greene, William H.; and Anderson, Melvin S.: Buckling Loads of Stiffened Panels Subjected to Combined Longitudinal Compression and Shear: Results Obtained with PASCO, EAL, and STAGS Computer Programs. NASA TP-2215, January 1984.

Table I. Design Constraints

Constraint	Requirement
panel length	30 in.
panel width	24 in.
buckling	panel does not buckle below design load
minimum thickness of outer ± 45 -degree plies	.0055 in.
maximum compressive or tensile strain	.006 in./in.
maximum shear strain	$\pm .01$ in./in.
minimum global axial stiffness	dependent upon design load (see ref. 3)
minimum global shear stiffness	dependent upon design load (see ref. 3)
corrugation angle, α (see fig. 1)	45 degrees
corrugation width, b (see fig. 1)	same for top and bottom
skins	same stacking sequence for top and bottom skins of sandwich panel

Table II. Material Properties

Material property	typical graphite-thermoplastic material	coupons and fabricated panels
Longitudinal Young's modulus, Msi	19.4	14.5
Transverse Young's modulus, Msi	1.29	.97
Shear modulus, Msi	.74	.55
Major Poisson's ratio	.38	.38
Specific Weight, lb/in. ³	.057	.057

Table III. Test Specimens

Specimen Designation	Skin Stacking Sequence	Corrugation Stacking Sequence	Corrugation Width ^a , in.	Panel Length, in.
Semi-Sandwich Panels				
A	$[(\pm 45)_2/\overline{90}]_s$	$[\pm 45/0_5/90/0_4/\pm 45]_s$	2.03	12.
B	$[(\pm 45)_2/0_4/90/\pm 45/0_2/90]_s$	$[\pm 45/0_6/\overline{90}]_s$	1.64	12.
C	$[(\pm 45)_3/0_2/90/(\pm 45)_2/0/\overline{90}]_s$	$[\pm 45/0_6/90/0_4/\overline{90}]_s$	1.54	24.
D	$[(\pm 45)_3/0_6/90_2/\pm 45/0_6/\pm 45]_s$	$[\pm 45/0_5/90/0_3]_s$	1.32	24.
Sandwich Panels				
E	$[(\pm 45)_2/\overline{90}]_s$	$[\pm 45/0_6/\pm 45/0_6/90]_s$	2.00	12.
F	$[(\pm 45)_2/\overline{90}]_s$	$[\pm 45/0_6/\pm 45/0_6/90]_s$	2.00	24.

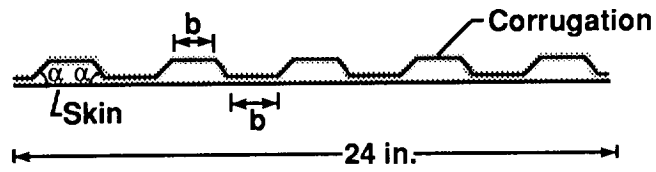
^a Corrugation width is b in figure 1.

Table IV. Optimum panels

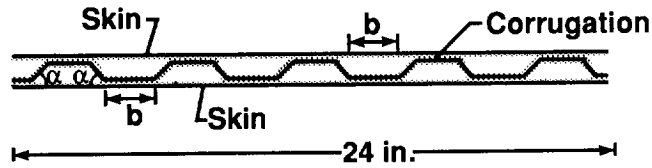
N_x/L , lb/in. ²	critical constraints ^a	corrugation width ^b , in.	skin thickness, in.	corrugation thickness, in.
Semi-Sandwich				
100	E, G, λ_{30}	1.82	.060	.112
250	E, G, λ_{30}	1.42	.145	.080
500	E, G, λ_1, λ_{15}	.98	.192	.084
800	G, $\lambda_1, \lambda_9, \lambda_{10}, \gamma$.77	.203	.125
Sandwich				
100	E, $\lambda_1, \lambda_{12}, \lambda_{13}$	1.88	.060	.049
250	E, $\lambda_1, \lambda_{15}, \lambda_{16}$	1.68	.041	.138
500	E, λ_1, λ_{15}	1.56	.056	.164
800	E, $\lambda_1, \lambda_{12}, \lambda_{13}, \lambda_{14}$	1.21	.077	.166

^a E is the extensional stiffness, G is the inplane shear stiffness, λ_i is the buckling mode with i axial half-waves, and γ is the inplane shear strain.

^b Corrugation width is b in figure 1.



a) Semi-sandwich panel



b) Sandwich panel

Figure 1. Panel design configurations.



a) Cross-section of panel A



b) Cross-section of panel E

Figure 2. Test specimens.

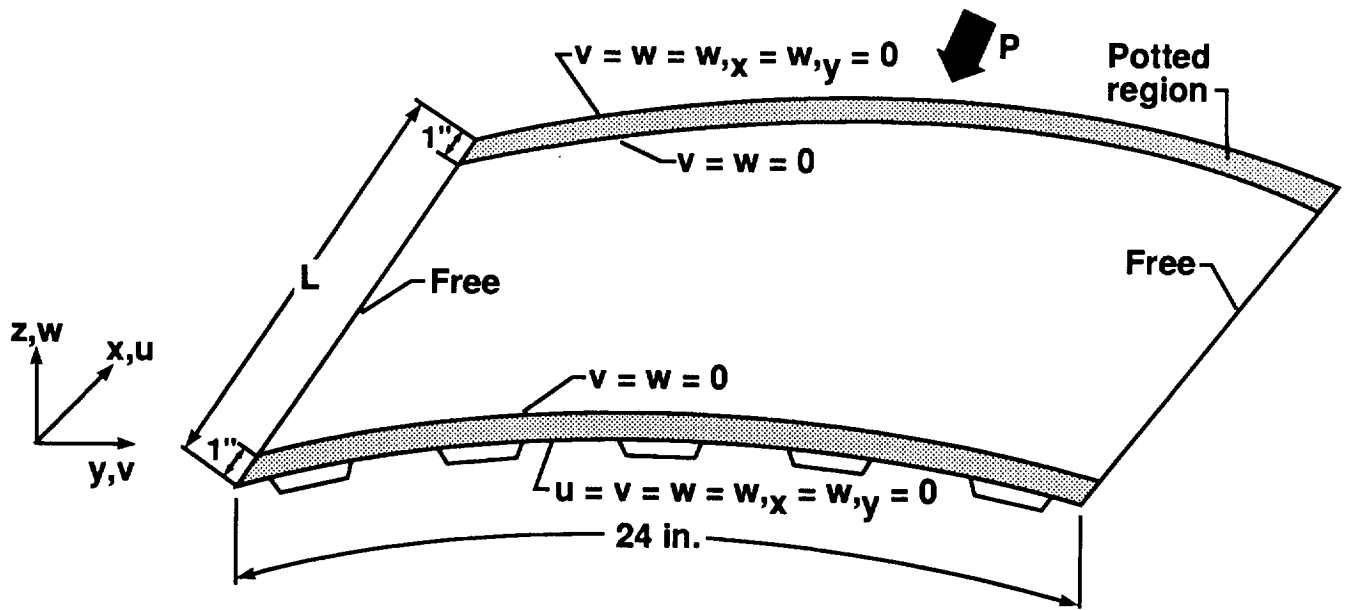


Figure 3. Finite element boundary conditions.

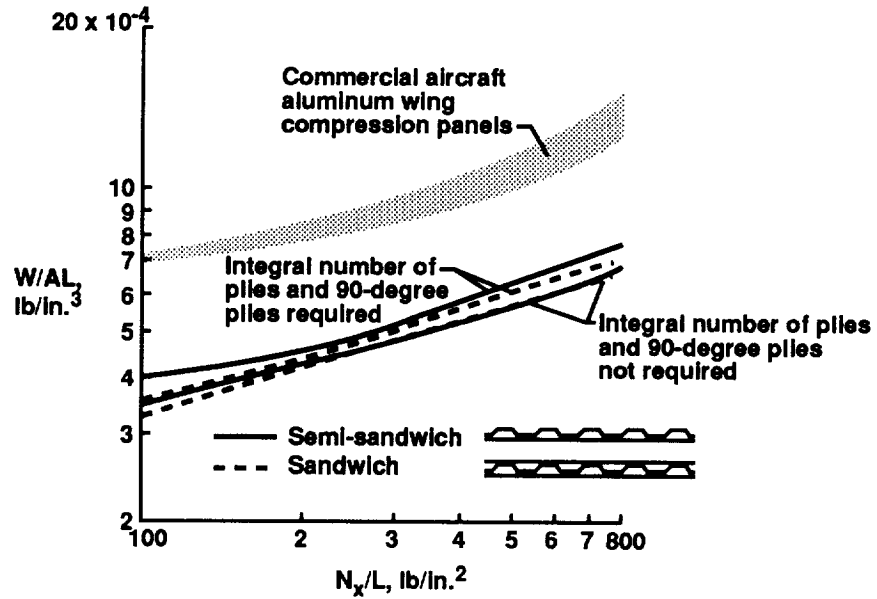


Figure 4. Structural efficiency of graphite-thermoplastic panels.

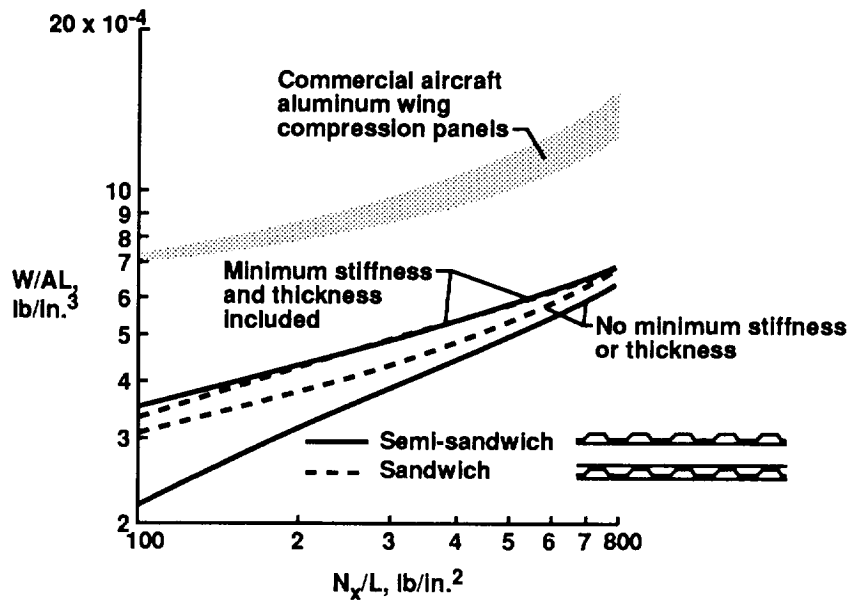


Figure 5. Effect of thickness and stiffness constraints on structural efficiency.

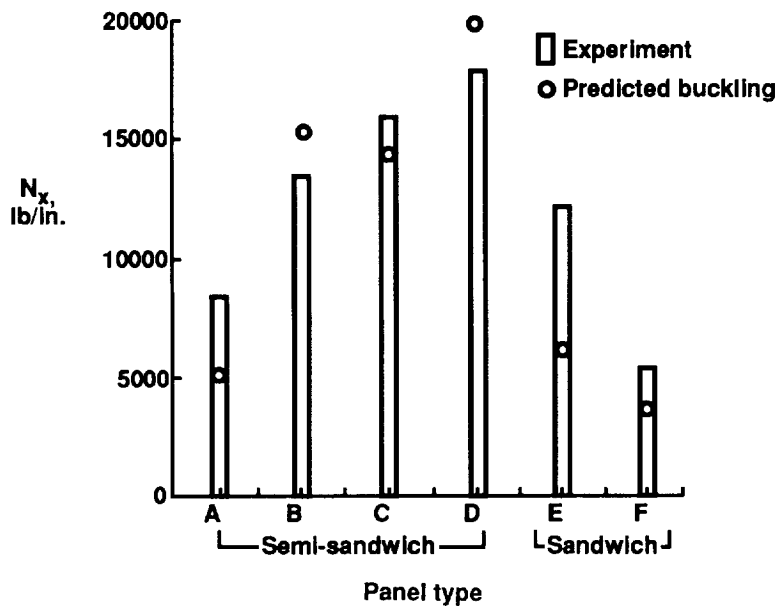


Figure 6. Stress resultants of control panels.

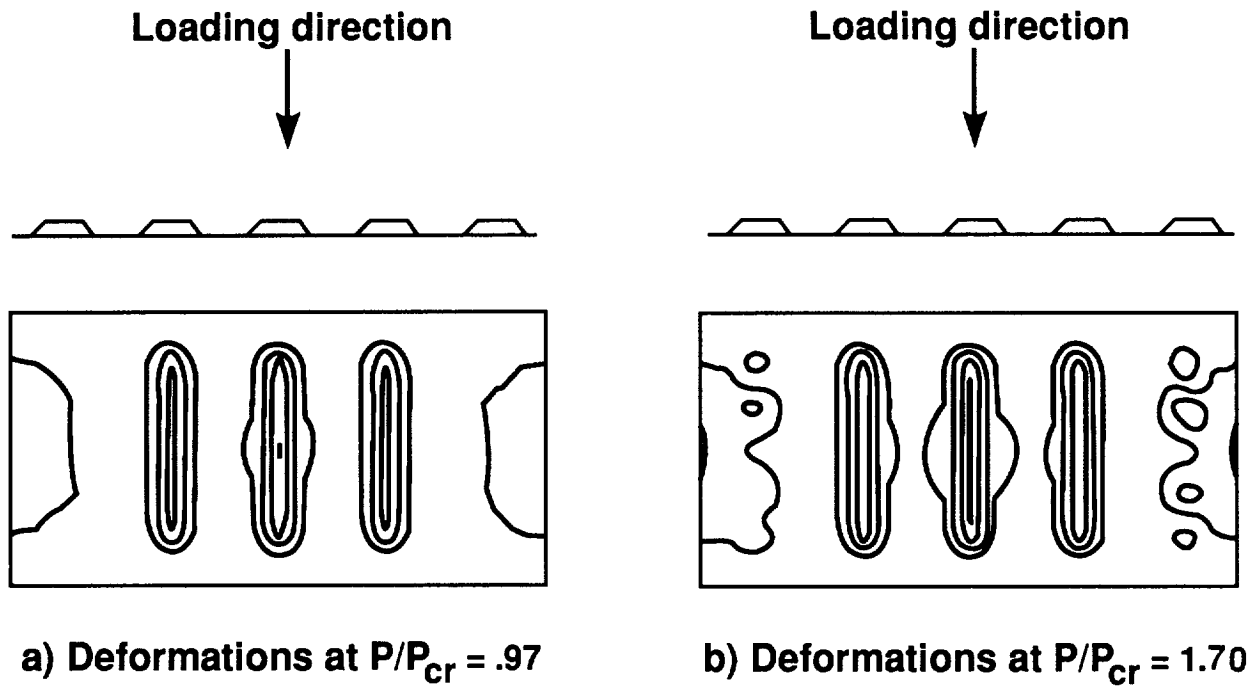


Figure 7. Analytically determined out-of-plane deformation of the skin of panel A.

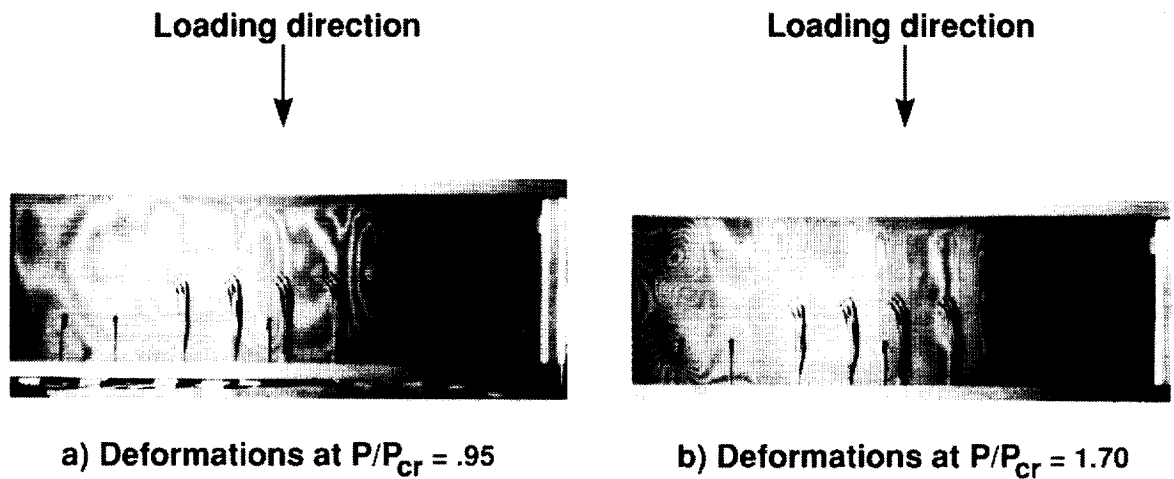


Figure 8. Moiré patterns of out-of-plane deformations of the skin of panel A.

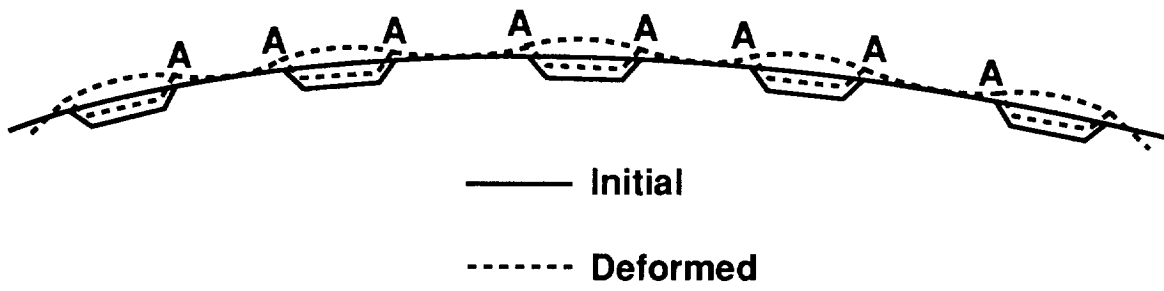


Figure 9. Sketch of deformation shape of semi-sandwich panel.

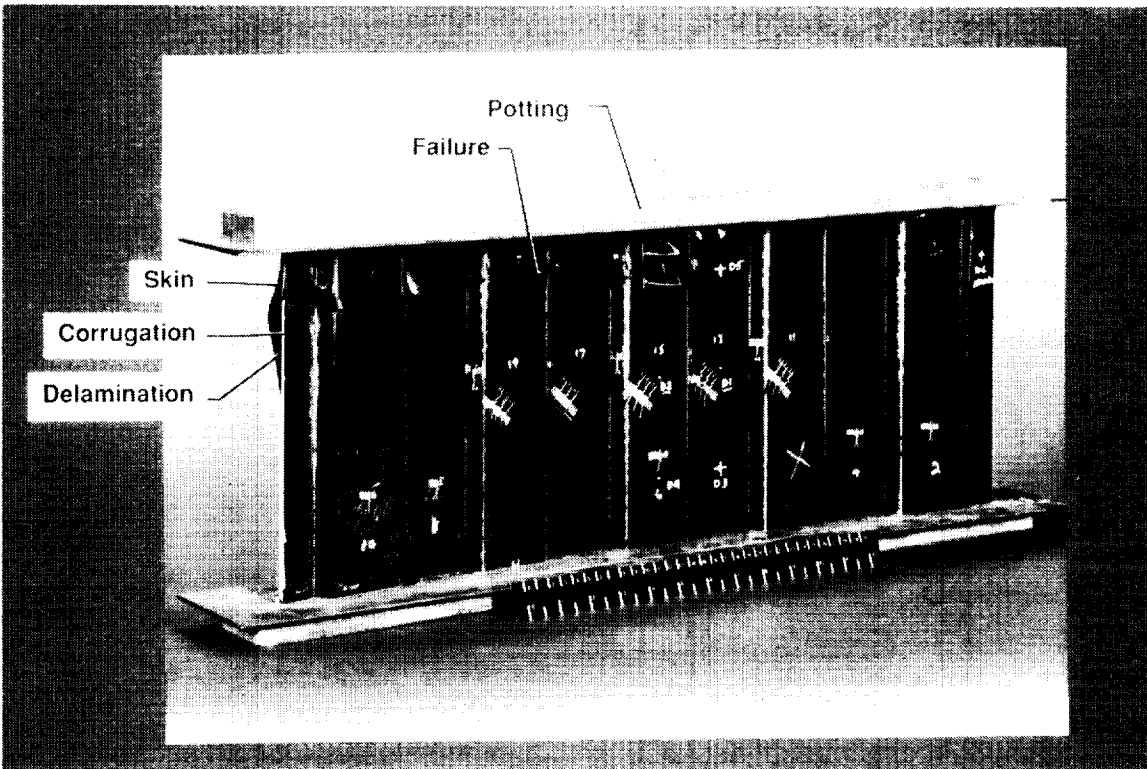


Figure 10. Panel A after failure.

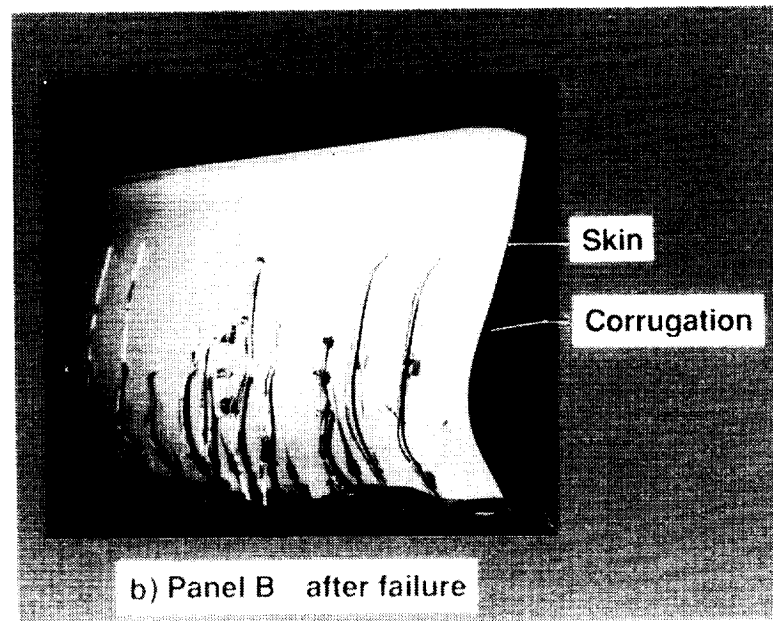
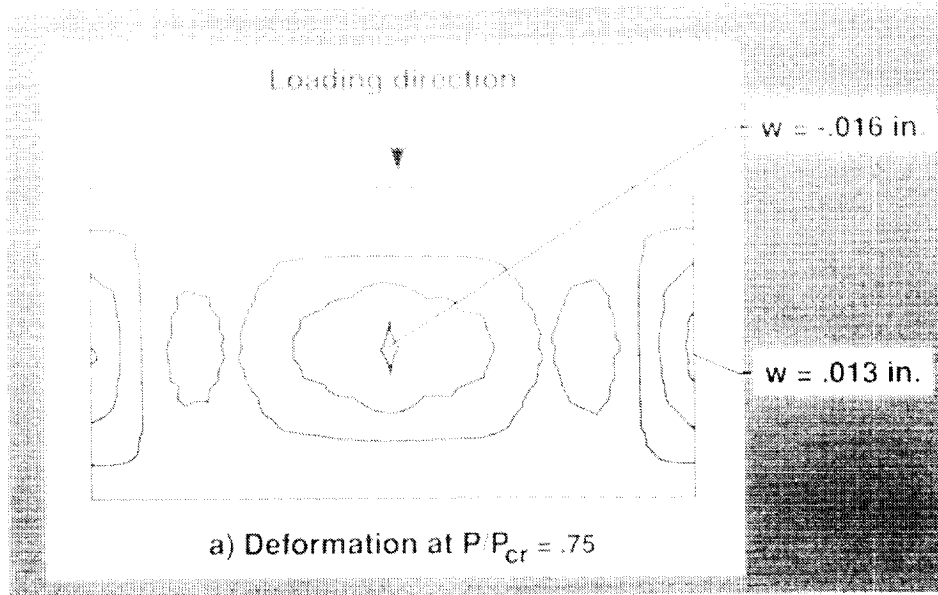


Figure 11. Deformations in panel B during and after loading.

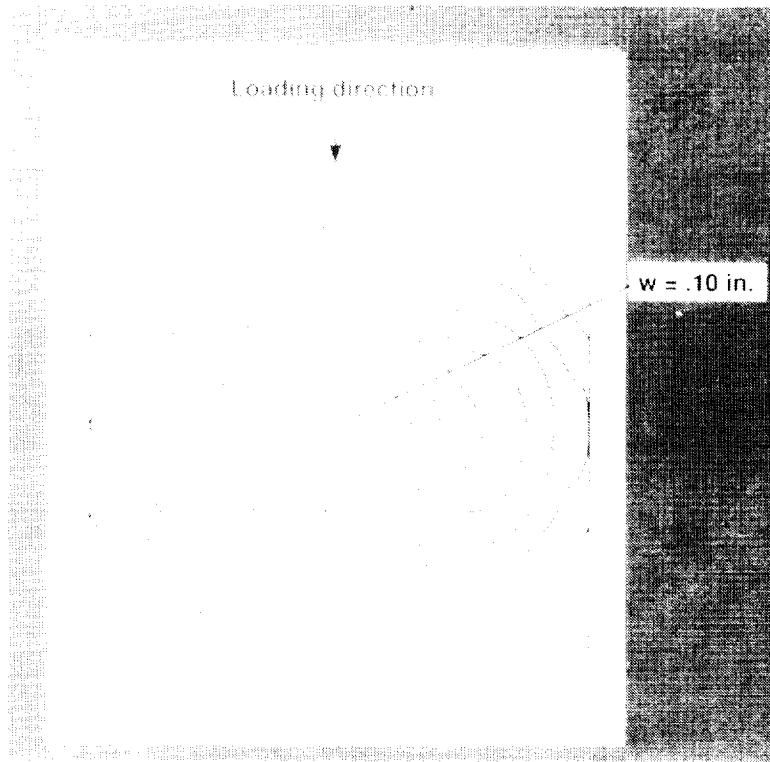


Figure 12. Deformations in panel C at $P/P_{cr} = .95$.

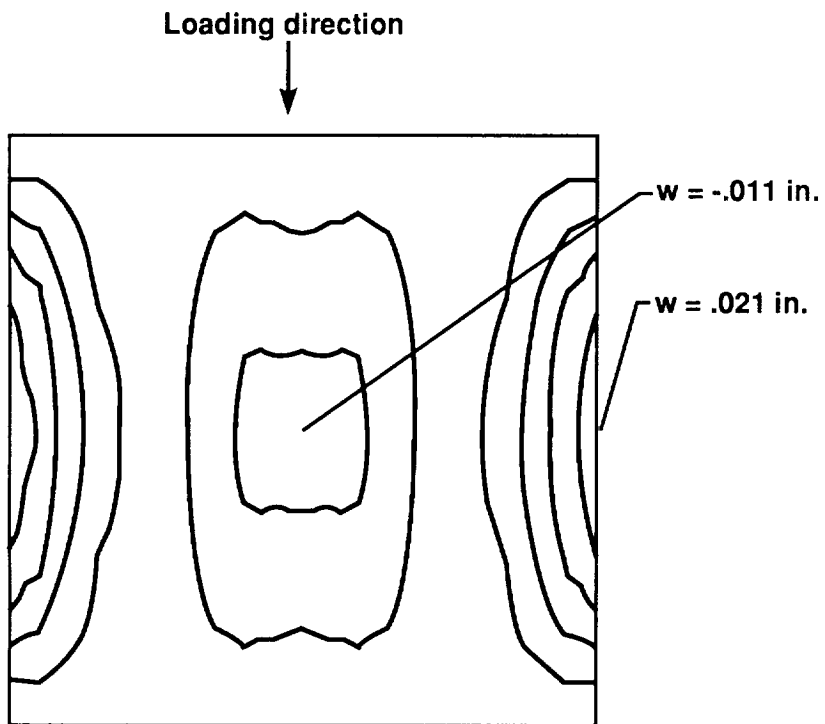
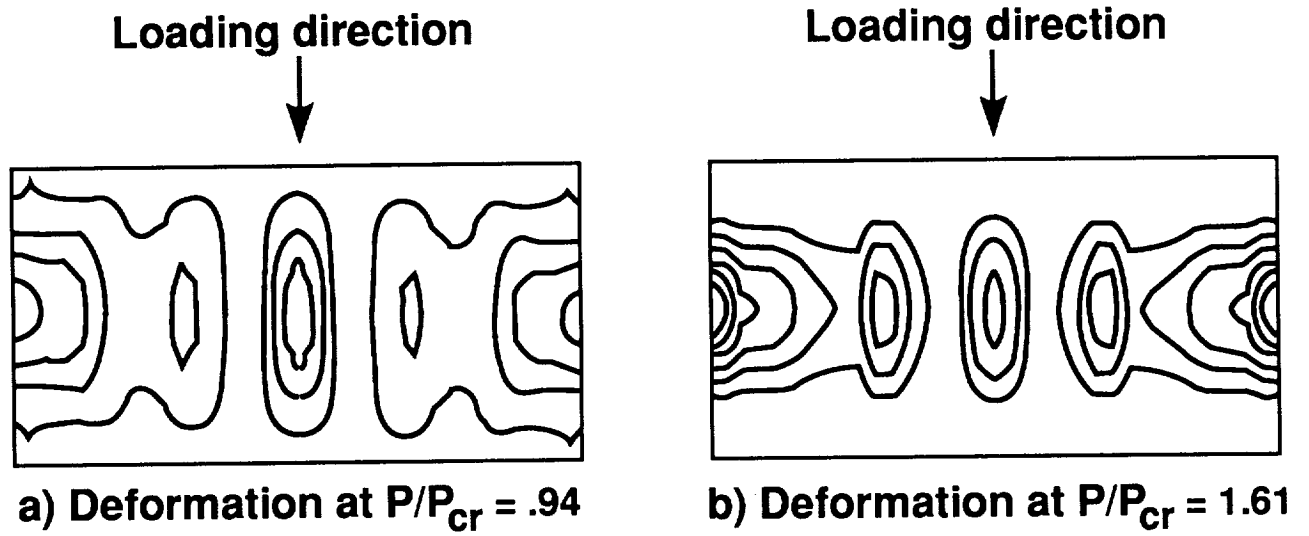


Figure 13. Deformations in panel D at $P/P_{cr} = .88$.



P/P_{cr}	w edge, in.	w center, in.
.94	.007	.004
1.61	.120	.060

Figure 14. Deformations of one skin of panel E during loading.